Author's Accepted Manuscript

Study on Seismic Behavior of Encased Steel Jacket-strengthened Earthquake-damaged Composite Steel-concrete Columns

Cheng-xiang Xu, Sheng Peng, Jie Deng, Chong Wan

Cite this article as: Cheng-xiang Xu, Sheng Peng, Jie Deng and Chong Wan, Study on Seismic Behavior of Encased Steel Jacket-strengthened Earthquake-damaged Composite Steel-concrete Columns, *Journal of Building Engineering,* https://doi.org/10.1016/j.jobe.2018.02.010

This is a PDF file of an unedited manuscript that has been accepted for publication. As a service to our customers we are providing this early version of the manuscript. The manuscript will undergo copyediting, typesetting, and review of the resulting galley proof before it is published in its final citable form. Please note that during the production process errors may be discovered which could affect the content, and all legal disclaimers that apply to the journal pertain.

Study on Seismic Behavior of Encased Steel Jacket-strengthened Earthquake-damaged Composite Steel-concrete Columns

Cheng-xiang Xu[a], Sheng Peng[a,*], Jie Deng[a], Chong Wan[b]

[a]Department of Civil Engineering, School of Urban Construction, Wuhan University of Science and Technology, Wuhan, 430065, P.R. China.
[b]School of Urban Construction, Yangtze University, Jingzhou, 434023, P.R. China.
*Corresponding author at: department of Civil Engineering, School of Urban Construction, Wuhan University of Science and Technology, Wuhan, 430065, China. Tel: 15623040982. pe_sh@sina.com (P. Sheng).

Abstract

In order to study the seismic behavior of earthquake-damaged composite steel-concrete columns strengthened by enveloped steel, based on current design codes, four composite steel-concrete column models were designed and manufactured. Destructive tests on the models under low-cyclic loading were then carried out. The feasibility and effectiveness of earthquake-damaged columns strengthened by enveloped steel and the reinforcement effect on different levels of seismic damage were studied. The results show that enveloped-steel-strengthened earthquake-damaged composite steel-concrete columns meet the strong column-weak beam requirement of seismic design, and the failure mode of all the columns was in bending. The performance of the rehabilitated columns can reach or even exceed the level of their original seismic performance before seismic damage. Composite steel-concrete frame columns strengthened by enveloped steel were also simulated using the finite element (FE) analysis software ABAQUS. The analytical study was conducted and compared with the experimental results, and it was basically consistent with the experimental data.

Keywords: composite steel-concrete column; encased steel jacket; seismic damage; finite element (FE) analysis; seismic behavior

Natation

The following symbols are used in this paper:

Δ_y is yield displacement;

P_y is yield load;

Δ_u is limit displacement;

P_u is ultimate load;

μ denotes ductility coefficient;

E denotes energy dissipation coefficient;

Δ_u^+ is positive ultimate;

Δ_y^+ is positive yielding displacement;

Δ_u^- is negative ultimate;

Δ_y^- is negative yielding displacement;

E_D is the total energy dissipated per cycle;

E_s is the elastic strain energy at the peak displacement per cycle;

f_c is the peak stress (MPa);

ε_0 denotes the strain corresponding to f_c;

E_c is young modulus of the concrete;

σ_t is the average tensile stress;

ε_t is the average tensile strain;

f_{cr} is the tensile cracking stress, which can be taken as $f_{cr}=0.31f_c^{0.5}$(MPa);

ε_{cr} is the cracking strain;

σ_{nom} is nominal stress;

ε_{nom} is strain values;

σ_{ture} denotes true stress(named as cauchy stress);

ε_{ture} is logarithmic strain;

K is strength enhancement coefficients;

Z_m denotes the slope of strain softening stage;

f_c is the peak stress of restraint concrete;

f'_c is the peak stress of unrestraint concrete;

ε denotes the peak strain values of restraint concrete;

ε_c is the peak strain values of unrestraint concrete;

ρ_{yh} denotes the stirrup ratio;

ρ_{jg} denotes the steel jacket ratio;

f_{yh} is the yield strength of stirrup;

f_{jg} is the yield strength of steel jacket;

h'_{yh} is the height of concrete core of original column;

h'_{jg} is the height of concrete core of strengthened column;

s_{yh} is the center spacing of stirrup of original column;

s_{jg} is the center spacing of stirrup of strengthened column.

1. Introduction

As a kind of attractive composite structure, steel reinforced concrete structure has the advantages such as high carrying capacity, high rigidity and good seismic performance. Steel reinforced concrete has been widely used in large-span structures and high-rise buildings in earthquake-prone areas around the world [1,2]. The recent earthquake survey of China's Wenchuan earthquake (2008), Iranian-Pakistani boundary earthquake (2013) and China's Ludian earthquake in Yunnan Province (2014) shows that a large number of damaged frame structures need damage grade identification and corresponding reinforcement & repair measures with the exception of critically damaged frames demanding turnover and reconstruction [3,4,5,6]. According to the principle, steel reinforced concrete frame composite column is an important load-bearing member of frame structure, therefore it is necessary to study restoration and reinforcement of steel reinforced concrete column as well as its anti-seismic property [7,8].

At present, "Standard for earthquake-resistant evaluation of buildings" (GB50023-2009), "Regulation of building seismic strengthening technique" (JGJ116-2009) and "Technical guide for post-earthquake building identification and reinforcement" have never focused on seismic identification and reinforcement of steel reinforced concrete structure. In particular, buildings designed in accordance with China's earthquake resistant code can still meet the requirement of "being modifiable in moderate earthquake and not falling in strong earthquake". For buildings that can be repaired, "reinforcement and repair" should be more reasonable than "turnover and reconstruction" either from the point of view of solving the urgency of settlement problem of the masses in the disaster areas or from the economic point of view of post-disaster reconstruction. Therefore, the study of seismic damage degree, reinforcement method and seismic performance of reinforced structure means very important engineering significance for improving its seismic

capacity and post-disaster recovery and reconstruction. Repair & reinforcement of seismic damage structure mainly involves three issues: (1) Repair seismic performance of the reinforced structure. (2) Influence and law of different degrees of earthquake damages on structural restoration and reinforcement. (3) The specific advantages of repaired and reinforced of structure over unreinforced structure. (4) Impact of different axial compression ratios [9], different reinforcement heights on structure seismic [10].

Encased steel jacket has excellent mechanical properties and convenient construction characteristics [11,12,13,14]. The design method is simple, construction operation is safe and effective, and the reinforcement effect is reliable; bending ability of the components can be reinforced based on actual needs to obviously improve strength and toughness, restore bearing capacity, and extend service life; steel plates are closely integrated with the original components as a whole through viscous material with strong binding capacity, to bear the load together, wherein the role of steel plate is like rebar inside the concrete; the concrete at the bonding parts of steel plate is subjected to constraints, which can control expansion of existing cracks and prevent crack generation. It has been widely used in seismic reinforcement projects [15].

In this cyclic loading test, four large-scale steel reinforced concrete columns were designed and fabricated on the basis of the existing steel reinforced concrete composite technical specification. The test specimen was subjected to simulated earthquake pre-damage, reinforcement of component with seismic damage, and post-reinforcement low cycle repeated load test. The seismic performance of encased steel jacket-strengthened steel reinforced concrete columns was evaluated. In addition, the test results were verified by finite element. Based on the verified numerical model, influence of different axial compression ratios and different reinforcement heights on seismic performance of steel reinforced concrete column with seismic damage was analyzed, and the results were in accordance with the actual engineering requirement.

2．Experimental program

2.1. General information and material properties of specimens

The bottom sections of ground floor frame column is selected as the test object. Based on the principle, four 1/2-scaled specimens, one original specimen (numbered SRC-0), one strengthened column (numbered WSRC-0) by steel jacket, and two columns were pre-damaged by different degrees to simulate moderate (numbered WSRC-1) and severe earthquakes (numbered WSRC-2) and strengthened by steel jacket, respectively. Specimen dimension and steel details are shown in Fig. 1. The test specimens had a rectangle cross section of 200mm×270mm. The cover thickness of the concrete specimens was kept at 25mm. In addition, the composite steel-concrete frame columns were short columns.

The data in Table 2 indicates that specimens SRC-0, WSRC-0, WSRC-1, WSRC-2 are under the same axial compression ratio, and have the same shear span ratio and concrete strength grade. Accordingly, they can be considered to have different degree of damage and strengthening level. Based on the same considerations, specimens WSRC-0~WSRC-2 are also considered to have same strengthening level of steel enveloped.
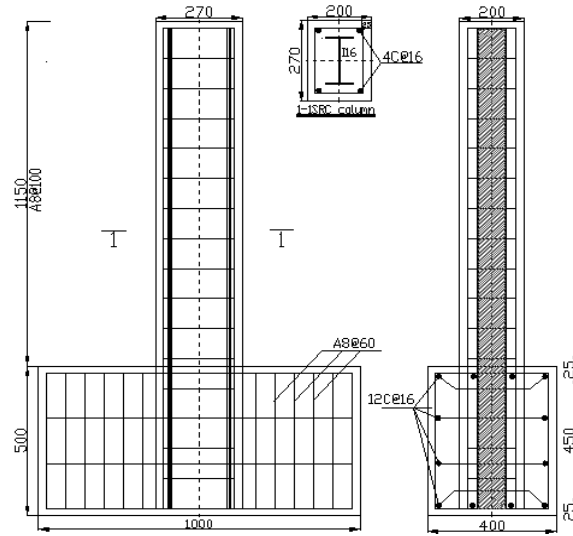
Fig .1. Specimen dimension and steel details Note: dimensions are in mm

Four $\phi16$ rebars were placed in each boundary zone of the specimens. The cross-section reinforcement ratio (ρl) of the specimens was 1.60% and the stirrup ratio (ρ_v) was 0.68%. The steel ratio (ρ_a) of the specimens was 4.84%.

To ensure the same quality of concrete, C40 commercial concrete was used, pouring from the same batch, with 28 days of maintenance. The concrete compressive strength was determined by the compression testing on standard cubic samples of the casted concrete on the day of specimen testing [16]. The compressive strength, f_c, was taken as 0.76 times the cubic compressive strength, f_{cu}, in accordance with the "Chinese code for design of concrete structures" (GB 50010-2010) [17]. Table 1 shows the material properties of the concrete, profile steel and stirrup obtained by tests.

Table 1. Material properties

Material	Specification	Yield strength f_y /MPa	Ultimate strength f_u /MPa	Elastic modulus E_s /MPa
concrete	150mm length cube	39.6	30.10	3.25×10^4
I16 profile steel	Q235B	264.5	405.8	2.01×10^5
longitudinal bar	HRB400	375.7	515.6	2.05×10^5
stirrup	HPB300	312.4	443.1	2.10×10^5

2.2. Pre-damaged and reinforcement of specimens

Four test specimens were fabricated in the test, of which one was prototype test specimen for contract (numbered SRC-0) without pre-damage and reinforcement treatment, one was enveloped in steel jacket-confined test specimen (numbered WSRC-0) without pre-damage but with reinforcement treatment, and two were enveloped in steel jacket-confined test specimens with pre-damage (numbered WSRC-1 and WSRC-2, respectively), to be respectively applied with 1/100, 1/50 displacement angle pre-damage. The reinforcement design was the same, and after the completion of the reinforcement, all the test specimens were loaded to the specified damage conditions according to the specified loading system before loading was stopped. After pre-damage of test specimen with 1/100 displacement angle, slight transverse cracks appeared within the range of column section breadth on both left and right sides of the test specimen (the specific orientation is

shown in Fig. 3 (a), but no obvious cracks were observed on the back side; transverse, vertical cracks appeared within column section breadth on left and right sides of test specimen with 1/50 displacement angle pre-damage, the transverse cracks slightly tilted and reached the back of the test specimen, but did not penetrate through. The reinforcement parameters of each test specimen are shown in Table 3. The enveloped steel jacket was welded by angle steel and steel plate. According to "Regulation of building seismic strengthening technique" (JGJ116-2009), the angle steel was selected as L63mm×4mm, steel plate was selected in two sizes, namely 240mm×60mm×4mm and 170mm×60mm×4mm, the angle steel, steel plate and concrete were filled with sticky steel glue, adjacent steel plate had a spacing of 150mm, with reinforcement height at 500mm. In view of the fact that the test specimen was pre-damaged, the enveloped steel jacket was not embedded in the column grade beam, because this may artificially increase degree of pre-damage and thus affect the test results. The enveloped steel jacket was connected to the grade beam only by the sticky steel glue at the bottom of the steel jacket. The reinforcement area of test specimen is shown in Fig. 2.

Table 2. Parameters of specimens

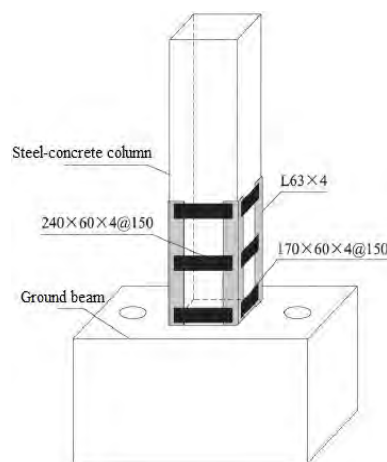| Specimen	Damage degree	Axial compression ratio (n)	Shear span ratio (λ)	Displacement angle	Angle steel	Strengthened level
SRC-0	Undamaged	0.32	3.33	—	4L63×4	no
WSRC-0	Undamaged	0.32	3.33	—	4L63×4	yes
WSRC-1	Moderate damaged	0.32	3.33	1/100	4L63×4	yes
WSRC-2	Severe damaged	0.32	3.33	1/50	4L63×4	yes

Fig. 2. Strengthened by steel jacket at column bottom

2.3. Test device and loading system

The columns were constructed and tested at the Civil Engineering Experiment Center of Yangtze University. Test set-up for cyclic loading test is shown in Fig. 3. The lateral load was applied by a servo-controlled hydraulic actuator at the upper column end, using a displacement-controlled tester at the speed of 10 mm/min. The specimens can be rigidly anchored to the ground through the ground beam which was placed at the bottom of the specimens. To realize the free displacement of the top end of the frame column behaving as a cantilever, the frictionless rollers were installed on the top of the hydraulic jacks. The hydraulic jacks were able to move freely in the horizontal direction so as to accommodate the lateral displacement of the specimen. The

upper end loading scheme was adopted to simulate the P-Δ effect caused by the applied axial compressive load acting on the lateral displacement of the columns. The vertical load is on the top of the column, whose size is 500 KN. The tests of the loading system followed the JGJ101-96 guidelines.
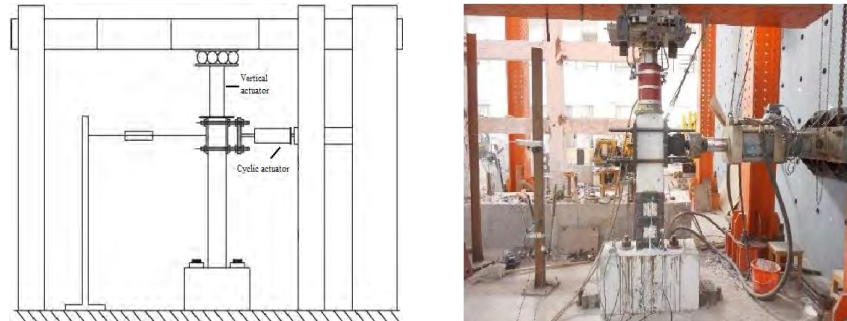

Fig. 3. Test set-up for cyclic loading test

Fig.4. shows the loading protocols of the test. The displacement amplitude for each level of loading was determined according to the estimated yielding displacement of numerical analysis before the test (Δ/L$\times$100%=1.0%). Prior to the displacement level of 0.25%, the displacement amplitude increment was 0.25% for one amplitude with one cycle to monitor the initial cracking point. Then the displacement amplitude increment was 1.0% with three cycles for each amplitude. The experiment was stopped when the load fell to 85% of the ultimate load, or when the specimens were unable to bear the axial force.
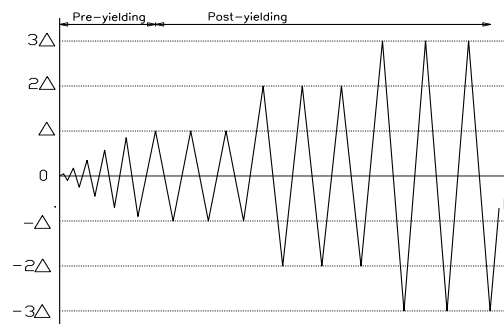
Fig. 4. Loading protocols of the test

Measurement contents: load-displacement at the end of column, strain of profile steel, stirrup, reinforcement and encased steel jacket. The load-displacement and strain were collected by the LETRY control system. The arrangement of strain gauge is shown in Fig. 5.
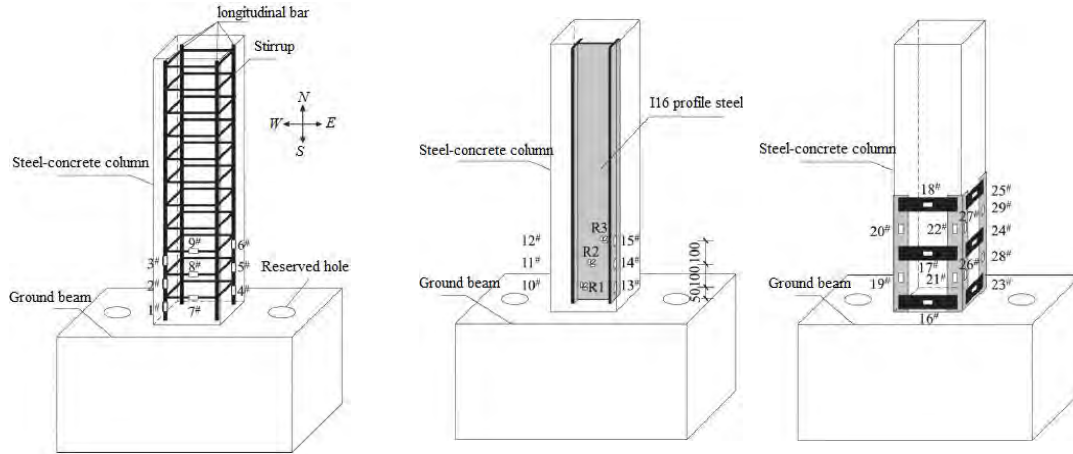
Fig. 5. Arrangement of strain gauge. (a) Longitudinal reinforcement and stirrups. (b) Profile steel. (c) steel enveloped

3. Failure modes and damage progression

The specimens were preloaded with the smaller displacement control before the test, followed by the specified loading series when data acquisition and display of detection equipment was normal. In order to correspond to the positive and negative cycles of the hysteresis curve, stipulate the tension as "+" and the thrust as "-".

Test specimen SRC-0 is a prototype for contrast. In the first loading-unloading process with displacement angle 2% (±18mm), when loading to +16mm, the loading curve slightly bent, longitudinal bar yielded, the transverse cracks appeared on the concrete surface on the tension side, and the longitudinal cracks appeared at the column angle. In the subsequent loading cycle, longitudinal bar of the other side yielded, and concrete cracks healed or reproduced in slow development. In the first loading-unloading process with displacement angle 3% (±27mm), when loading to -23mm, the thrust of the actuator reached the peak value, and the flange yielded. In the continued loading, cracks gradually increased, and the vertical cracks of the column angle were inclined to the column center. In loading cycle with displacement angle (±36mm), transverse, vertical crack width increased, continued to develop to the column center, forming through cracks. In the first loading cycle with displacement angle 5% (±45 mm), the concrete around column angle cracks shed under the action of reciprocating cycle, with unloading curve more inclined. In the first loading cycle with displacement angle 6% (±54mm), the width of through crack was significantly expanded, the concrete of column angle broke away from the main body, the test specimen reached the set destruction standard, then stop the test after completion of the loading test. Destruction phenomenon of the test is shown in Fig. 6 (a).

Test specimen WSRC-0 is an undamaged comparative test specimen. In the first loading cycle with displacement ±18mm, at displacement of -17mm, the longitudinal bar yielded, while in the second loading cycle, the offside longitudinal bar yielded. In the first loading cycle with displacement ±27mm, at displacement of -25mm, the reciprocating load reached the peak, the flange yielded, while in the second cycle, the transverse cracks appeared in concrete which was not wrapped by encased steel. In the loading cycle with displacement ±36mm, the number of cracks

increased under the action of bending shear, the cracks crazed or closed in the push-and-pull, and cracks appeared on the sticky steel glue at the bottom of the column. In the third loading cycle with displacement ±45mm, at displacement of -40mm, the crack width of sticky steel glue at the bottom of the column was obviously increased, and the transverse cracks intersected to form through cracks at the breakage sound of the concrete. In the loading cycle with displacement ±54mm, sticky steel glue broke away from the bottom of the column, but the bearing capacity could be maintained. In the loading cycle with displacement ±63mm, at displacement of -58mm, the sticky steel glue fractured, and with the continuing load, the encased steel broke away from grade beam at the bottom of the column, the bearing capacity decreased to minus 85%, and finally the test specimen was broken. Destruction phenomenon of the test is shown in Fig. 6 (b).

Test specimen WSRC-1 was moderately damaged (1/100 displacement angle pre-damage). In the first loading cycle with displacement ±18mm, at displacement of +16mm, cracks appeared on the concrete which was not wrapped by encased steel at the bottom of the column, while the 1#, and 4# strain value overflowed, and longitudinal bar yielded. In the loading cycle with displacement ±27mm, the cracks continued to increase, the brittle sound of sticky steel glue at the bottom of the concrete was heard, 10# strain gage exceeded yield strain and the flange yielded. In the loading cycle with displacement ±36mm, the transverse cracks continued to increase. In the first loading cycle with ±45mm, at displacement of -38 mm, the crack width of sticky steel glue at the bottom of the column increased. During the subsequent loading process, the transverse crack width of the concrete increased, leading to penetrating causing through cracks. In the loading cycle with displacement ±54mm, the sticky steel glue ruptured, the encased steel broke away from the bottom of the column. In the first loading cycle with displacement ±63mm, at displacement of -53mm, the test specimen reached the intended damage condition, striking the batten plate at the bottom of the column, and the test specimen broke with hollowing sound. Destruction phenomenon of the test is shown in Fig. 6 (c).

Test specimen WSRC-1 was heavily damaged (1/50 displacement angle pre-damage). In the first loading cycle with displacement ± 18mm, at displacement of -16mm, the brittle sound of sticky steel glue could be heard at the bottom, and 1#, 4# strain gage successively reached the yield strain. In the loading cycle with displacement ±27mm, slight transverse cracks appeared on concrete which was not wrapped by encased steel at the bottom of the column. In the first loading cycle with displacement ±36mm, 10# strain value overflowed, the number of cracks increased, and transverse cracks were slightly inclined to the column center. In the first loading cycle with displacement ±45mm, the transverse cracks gradually penetrated, and the crack width of sticky steel glue widened with continuous brittle sound. In the first loading cycle with displacement ±54mm, at displacement of -51mm, the sticky steel glue ruptured, but the bearing capacity could be maintained. In the first loading cycle with displacement ±63mm, transverse cracks were penetrating through, therefore, it was unable to continue to bear, and the test specimen broke. Destruction phenomenon of the test is shown in Fig. 6 (d).
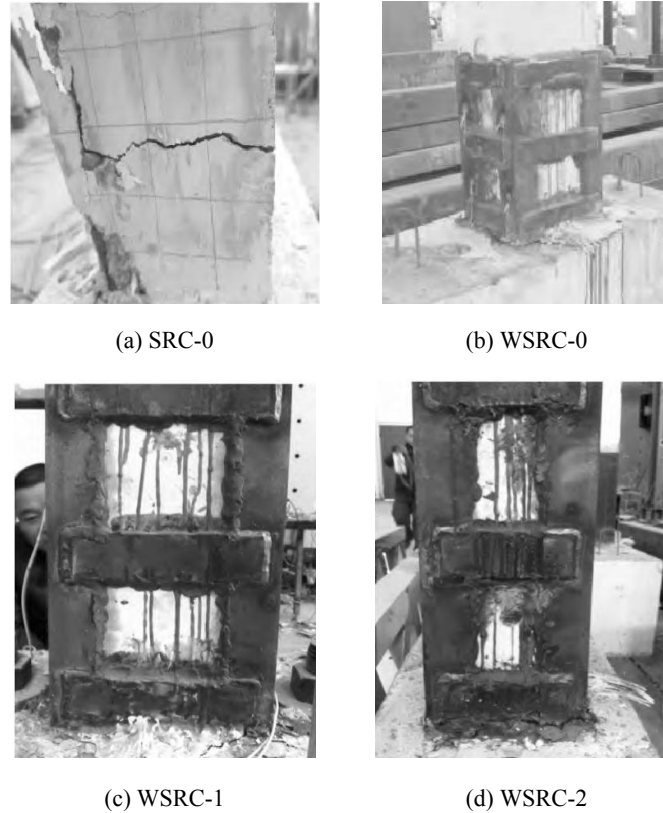
(a) SRC-0   (b) WSRC-0

(c) WSRC-1   (d) WSRC-2

Fig. 6. Failure modes of specimens

4. Experimental results and discussions

4.1. Hysteretic curve and skeleton curve

The load-displacement curve at the loading point of measured column-end horizontal load of test specimen SRC-0 and test specimen WSRC-0~WSRC-2 are shown in Fig.7. The hysteresis curves are similar and full in shape, with characteristics as follows: (1) the loading and unloading curves are almost straight and the hysteresis loop is not obvious before the horizontal loading displacement is loaded to the yield displacement. (2) In the reciprocating loading of the test specimen after yield, for the loading series at the same level, the stiffness of test specimen stiffness decreased with the increase of loading times, residual deformation increased, energy dissipation capacity declined, and test specimen damage accelerated. (3) After the peak load, displacement increased faster than the load, the loading-unloading curve became steeper, suggesting that the test specimen entered plastic development stage. (4) As can be known from Table 3, compared with SRC-0, ultimate loads of WSRC-0, WSRC-1 and WSRC-2 are increased by 23.0%, 12.9% and 7.4%, respectively, with ultimate displacement increased by 23.7%, 12.4%, 8.0% respectively.
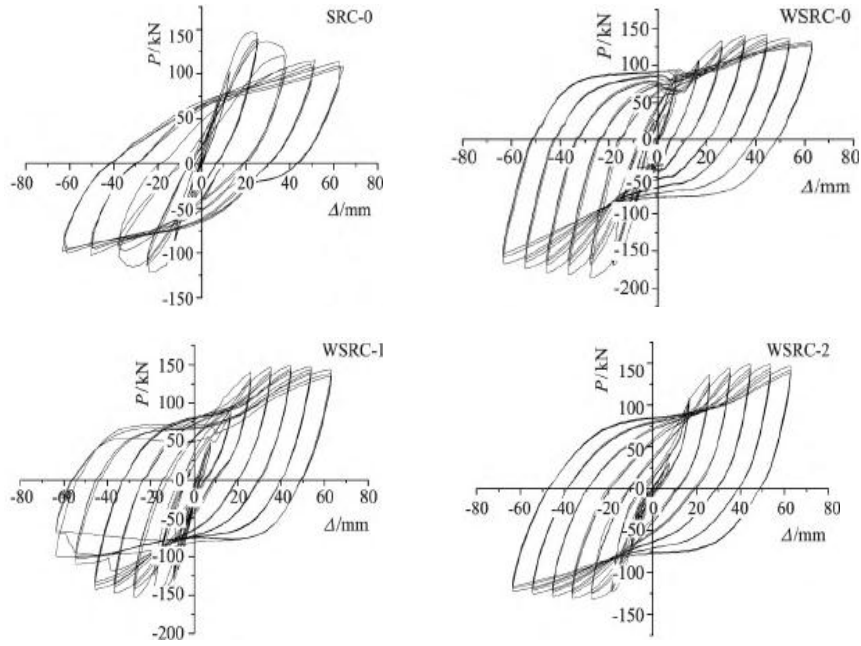
Fig .7. Hysteretic loops of specimens

Table 3. Characteristic points of skeleton curves

Specimen	Load direction	P_y/kN	Δ_y/mm	P_u/kN	Δ_u/mm	$\mu=\Delta_u/\Delta_y$	E
SRC-0	Positive	16.45	117.43	47.67	131.00	2.89	0.44
	Negative	-16.89	-119.11	-48.03	-133.01		
WSRC-0	Positive	17.36	140.19	58.99	161.14	3.40	0.53
	Negative	-17.41	-141.88	-59.17	-162.92		
WSRC-1	Positive	16.64	126.82	53.58	148.04	3.22	0.49
	Negative	-16.34	-124.12	-53.08	-143.89		
WSRC-2	Positive	16.60	121.09	51.46	140.80	3.10	0.46
	Negative	-16.27	-119.87	-50.21	-38.76		

Fig.8. shows the skeleton curve of specimens. The yield and limit points were determined as shown in Fig.9. The displacement between intersection of maximum force horizontal line and straight line passing through the origin and intersection of 85% ultimate load on the envelope curve, which is defined as yield displacement. The displacement corresponding to 15% ultimate load on the descending section of the envelope curve, which is defined as ultimate displacement.
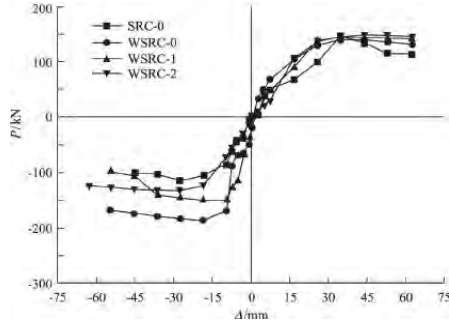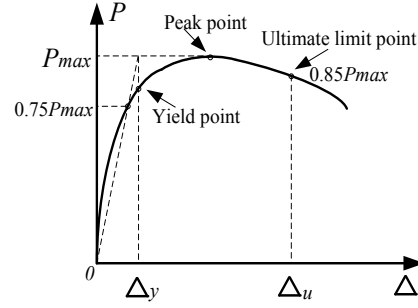
Fig .8. Skeleton curve of specimens

Fig .9. Definition of yield point and failure point

The displacement ductility coefficient, μ, was used to evaluate the deformation capacity of the specimens, which is defined as follows:

$$\mu = \frac{\left|\Delta_u^+\right| + \left|\Delta_u^-\right|}{\left|\Delta_y^+\right| + \left|\Delta_y^-\right|} \tag{1}$$

where Δ_u^+ and Δ_y^+ are the positive ultimate and yielding displacement, respectively; Δ_u^- and Δ_y^- are the negative ultimate and yielding displacement, respectively.

Table 4 lists the bearing capacity, deformability and ductility coefficient of the four critical moments of the 4 test specimens. It is found that the average ultimate bearing capacities of test specimen WSRC-0~WSRC-2 are increased by 19.25%, 6.09% and 1.87%, respectively in the positive and negative loading direction, the average limit displacements are increased by 23.50%, 11.45% and 6.25%, and ductility coefficients are increased by 17.64%, 11.41% and 7.27%. (1) After test specimen WSRC-0 is reinforced with encased steel jacket, the ductility coefficient is increased by 17.6%, which means that encased steel jacket can effectively improve ductility of frame column. (2) Ductility coefficients of test specimens are increased under different damage degree, the increasing rates of ductility coefficients of test specimen WSRC-1 and WSRC-2 are lowered to 11.4% and 10.4% ,respectively, the increasing rate decreases with the increase of damage degree. (3) Ductility coefficient of pre-damaged reinforcement test specimen is higher than that of prototype test specimen SRC-0, indicating that reinforcement with cased steel jacket can effectively restore ductility of damaged test specimen.

4.2. Energy dissipation

In order to quantify energy dissipation of the test specimen, the concept of equivalent damping coefficient is introduced, which is defined as the first cycle of displacement at each stage:

$$r = \frac{E_D}{2\pi E_s} \times 100\% \tag{2}$$

where E_D is the total energy dissipated per cycle; E_s is the elastic strain energy at the peak displacement per cycle. The definition of E_D and E_s are illustrated in Fig. 10.
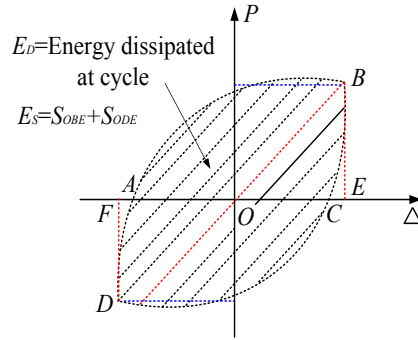
Fig. 10. Definition of E_D and E_s

Fig. 11 shows variation of equivalent damping coefficient of the four test specimens. In general, as the displacement increases, equivalent damping ratio of each test specimen increases gradually. In the whole process, equivalent damping ratio observes in the order of WSRC-0, WSRC-1, WSRC-2 and SRC-0 from large to small. Specifically, equivalent damping coefficient of encased steel jacket-strengthened steel reinforced concrete column is larger than that of unstrengthened steel reinforced concrete column, and the more severe the damage degree is, the smaller the equivalent damping coefficient is. Of four specimens, equivalent damping coefficients of test specimen WSRC-0 and WSRC-1 vary more significantly with the displacement.
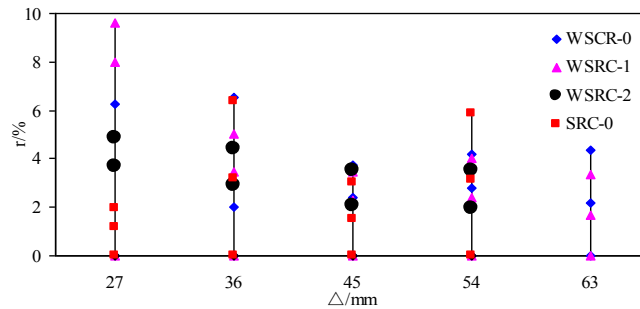
Fig. 11. Equivalent damping ratio

It can be seen from Table 4 that energy dissipation capacity of encased steel jacket-strengthened test specimen increases to some extent, with energy dissipation coefficient increased by 20.45%, 11.36% and 4.55% respectively. Wherein, WSRC-0 has the largest increase, while WSRC-2 energy dissipation capacity recovers and exceeds that of prototype contrast test specimen.

4.3. Strength and stiffness degradation

Figure 12 shows the stiffness degradation of the test specimen, which is assessed by secant stiffness, i.e., the average value of 3 cyclic loading peak values at the same level and displacement value corresponding to the peak value. As the displacement increases, the stiffness of the test specimen degrades significantly. Compared with SRC-0, the stiffness degradation of encased steel jacket SRC-0~SWRC-2 is slower, indicating that encased steel jacket reinforcement can well increase rigidity of test specimen.
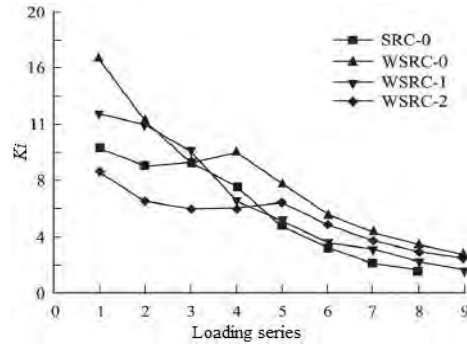
Fig. 12. Stiffness degradation curves of specimens

Fig. 13 shows bearing capacity degradation of the test specimen. It can be seen from Figure 13 that, the bearing capacity curve of test specimen SRC-0 changes greatly, with significant ups and downs, while that of pre-damaged test specimen is more stable and smooth.
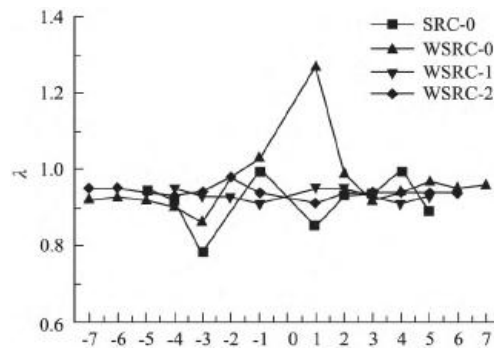

Fig. 13. Bearing capacity degradation curves of specimens

4.4. Strain analysis

Fig .14 shows the load-strain curve of the steel survey point R2[#], wherein, the strain is the average strain of survey point R2[#].

As can be seen from Fig .14, the strain of the steel increases with the load, indicating that the steel plays a role in the process of resistance to failure. The average strain size observes in the order of SRC-0, WSRC-2, WSRC-1 and WSRC-0 from large to small, which indicates that reinforcement with encased sleeve jacket can increase resistance of the test specimen to deformation and the resistance gradually reduces with increase of seismic damage degree. There are many rings in the load-strain curve at unloading, indicating that there is residual deformation during low-cycle repeated loading.
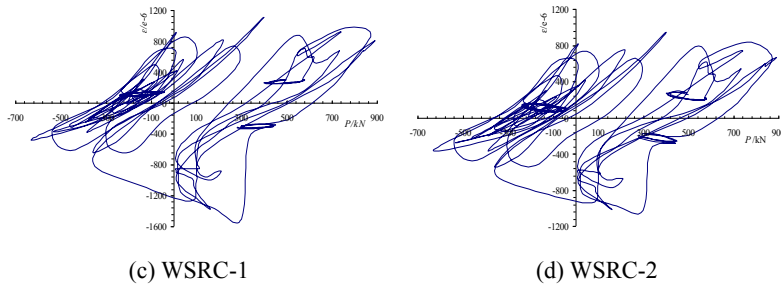

| (a) SRC-0 | (b) WSRC-0 |

(c) WSRC-1　　　　　　　　　　(d) WSRC-2
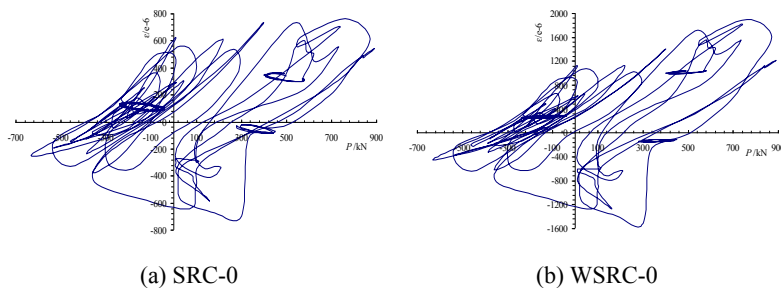
Fig. 14. *P-ε* curve of specimens

5. Numerical analysis

5.1. Finite element model

5.1.1. Element types and meshing

The FE model was built using the program ABAQUS. The earthquake-damaged composite steel-concrete frame column is strengthened by steel jacket through the four angles of the rectangular column. The angle steel and the plate steel are welded to form an encased steel jacket. The eight-node brick element with three translational degrees of freedom at each node (C3D8R) is used to model the concrete, angle steel, plate steel, and profile steel. Longitudinal bar and stirrups are dual-node truss element (T3D2). To determine the suitable element size with less computational time, the study of mesh refinement was conducted. The maximum size of the element less than 50 mm was chosen, due to the insensitivity of mesh refinement to model the steel buckling.

5.1.2. Loading, boundary conditions, and interactions

To apply the load on the specimen, the loading beam was described using with large stiffness at the top of the specimen. A reference point in this model was defined to assign the axial load, and the loading on the beam was uniformed distribution. The displacement-controlled loading was implemented on the reference point during the experimental procedure. The material models and element types of the foundation were same to those of the column. Boundary conditions of the model and that of the testing are consistent, and the column bottom restrains the freedom of translational motion and the trotational motion on the direction of X, Y, Z to simulate the base binding effect of capitals placed on the rigid plate. Plate and capitals are using bind (tie) connection.

Interaction on the contact surface between profile steel and concrete are mainly normal and tangential whose spring elements were set as Spring 2. Spring stiffness in the tangential should be set according to the bond strength, and that in the normal direction is infinite. To ensure the deformation compatibility between the steel and the concrete, welding enough shear studs on the profile steel in this test. Accordingly, the bond-slip between the concrete and steel was ignored in this study. Fig. 15 shows the finite element model.
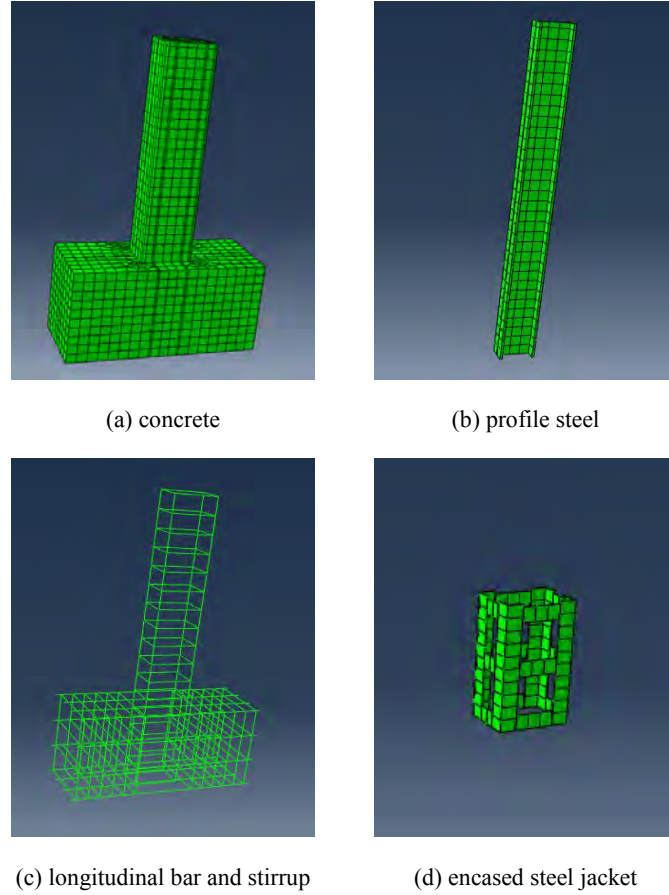
(a) concrete

(b) profile steel

(c) longitudinal bar and stirrup

(d) encased steel jacket

Fig.15. Finite element model

5.1.3. Material model of concrete and steel

A damage plasticity model can be used to describe the mechanical behavior of concrete. The program ABAQUS was adopted to build a damage plasticity model of concrete. This model required definition of the material's uniaxial constitutive relationships and the damage parameters. The compressive stress-strain model proposed by Popovics [17] was described, given by.

$$f_c' = \frac{n(\varepsilon_c/\varepsilon_0)}{n-1+(\varepsilon_c/\varepsilon_0)^{nk}} \cdot f_c \tag{3}$$

where f_c is the peak stress (MPa); ε_0 denotes the strain corresponding to f_c; and n and k are parameters determined by the following equations:

$$n = 0.8 + \frac{f_c}{17} \tag{4}$$

$$k = \begin{cases} 1.0 & \varepsilon_c/\varepsilon_0 \leq 1 \\ 0.67 + \dfrac{f_c}{62} & \varepsilon_c/\varepsilon_0 > 1 \end{cases} \tag{5}$$

To simulate the load transfer between cracks through the rebar, the effects associated with the rebar-concrete interface were modeled approximately by introducing tension stiffening into the tensile stress-strain relationship of the concrete. The average stress-strain model proposed by Belarbi and Hsu [18] was adopted as follows:

$$\sigma_t = \begin{cases} E_c \varepsilon_t & \varepsilon_t \leq \varepsilon_{cr} \\ f_{cr} \cdot \left(\dfrac{\varepsilon_{cr}}{\varepsilon_t} \right) & \varepsilon_t > \varepsilon_{cr} \end{cases} \tag{6}$$

where E_c is young modulus of the concrete; σ_t is the average tensile stress; ε_t is the average tensile strain; f_{cr} is the tensile cracking stress, which can be taken as $f_{cr}=0.31f_c^{0.5}$(MPa); and ε_{cr} is the cracking strain.

To predict the compressive and tensile damage in the cyclic loading, the uniaxial compressive damage variable and the tensile damage variable proposed by literature Birtel and Mark was described [19], given by. Fig. 16 shows the compressive and tensile stress-strain relationships of the concrete tasted at the part of the columns.

The nominal stress and strain values can be derived from the nominal stress and strain[20] by using the following equation:

$$\sigma_{ture} = \sigma_{nom}(1 + \varepsilon_{nom}) \tag{7}$$
$$\varepsilon_{ture} = \ln(1 + \varepsilon_{nom}) \tag{8}$$

where σ_{nom} is nominal stress; ε_{nom} is strain values; σ_{ture} denotes true stress(named as cauchy stress); ε_{ture} is logarithmic strain. σ_{ture} and ε_{ture} were used in the present FE model.

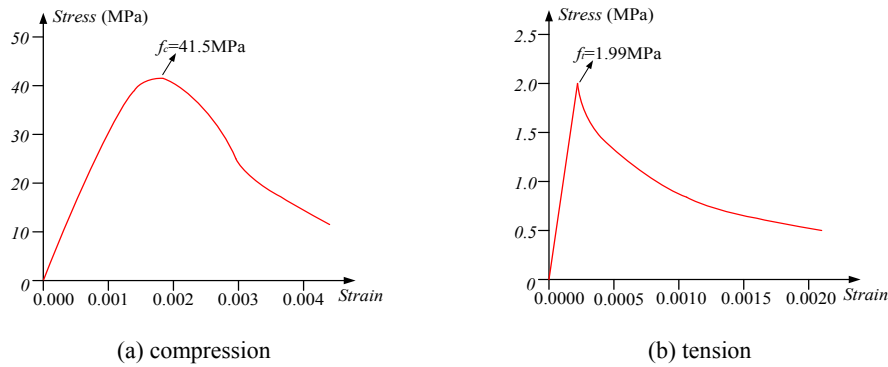(a) compression   (b) tension

Fig. 16. Stress-strain relationships of the concrete casted at the part of columns

The concrete compression section of enveloped-steel-strengthened column is improved by the Kent-Scott-Park model in the literature [21], given by.

$$f_c = Kf_c' \left[\frac{2\varepsilon_c}{0.002K} - \left(\frac{\varepsilon}{0.002K} \right)^2 \right] \qquad \varepsilon \leq 0.002K \tag{9}$$

$$f_c = Kf_c' [1 - Z_m(\varepsilon_c - 0.002K)] \geq 0.2Kf_c' \qquad \varepsilon > 0.002K \tag{10}$$

where K is strength enhancement coefficients; Z_m denotes the slope of strain softening stage.

Based on the Kent-Scott-Park version [22], the expression of strength enhancement coefficients, K, of concrete and the slope of strain softening stage, Z_m, are parameters determined by the following equations:

$$K = 1 + \rho_{yh} \frac{f_{yh}}{f_c'} + \rho_{jg} \frac{f_{jg}}{f_c'} \tag{11}$$

$$Z_m = \left[2\left(\frac{3+0.29 f_c'}{145 f_c' - 1000} \right) + 1.5\left(\rho_{yh}\sqrt{\frac{h_{yh}''}{s_{yh}}} + \rho_{jg}\sqrt{\frac{h_{jg}''}{s_{jg}}} \right) - 0.002K \right]^{-1} \tag{12}$$

where f_c is the peak stress of restraint concrete; f_c' is the peak stress of unrestraint concrete; ε denotes the peak strain values of restraint concrete; and ε_c is the peak strain values of unrestraint concrete. ρ_{yh} denotes the stirrup ratio; ρ_{jg} denotes the steel jacket ratio; f_{yh} is the yield strength of stirrup; and f_{jg} is the yield strength of steel jacket. h'_{yh} is the height of concrete core of original column; h'_{jg} is the height of concrete core of strengthened column; s_{yh} is the center spacing of stirrup of original column; and s_{jg} is the center spacing of stirrup of strengthened column.

The profile steel is analyzed by the classical ideal elastic-plastic model [23]. The stress-strain relationship of profile steel is shown in Fig. 17.
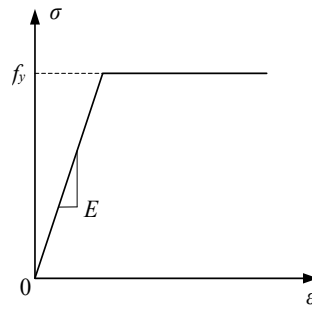

Fig .17.   Stress-strain relationship of profile steel

## 5.2. Analysis results and validation

It was found that force-displacement skeleton curve obtained by finite element analysis was basically consistent with the experimental results, as shown in Figure 18. In the finite element model, all the section steel, rebars and stirrups are buried in concrete. It is effective to simulate the nonlinear behavior of encased steel jacket-strengthened steel reinforced concrete columns with less computational time. In the finite element results, the stiffness of specimen is improved. This is mainly due to the inaccurate setting of boundary condition, the ignorance of the deformation of connecting rod in the foundation, the bias between simulated material properties and the actual performance, and full contact between steel and concrete. Fig. 19 shows comparison of concrete failure modes between finite element analysis and test results. The failure mode of finite element analysis is in good agreement with the test results. For unreinforced columns, concrete strain mainly occurs in plastic hinge area of the column, which is consistent with the test results. During the test, the column foot was crushed. For reinforced column, due to the restraint of cased steel jacket, the deformation of concrete tends to be uniform in the reinforcement range, and the maximum strain appears at the reinforcement boundary. In the test, penetrating diagonal crack was also found at the boundary of the reinforcement, and the simulation phenomenon was the same as the experimental phenomenon. The failure modes of section steel, encased steel in finite element analysis are shown in Fig. 20. The effect of reinforcement of encased steel jacket on the section steel is limited, as it is difficult to deform itself.
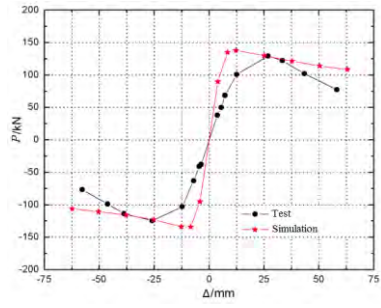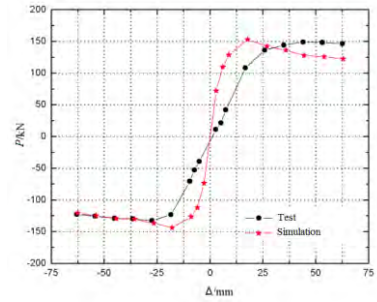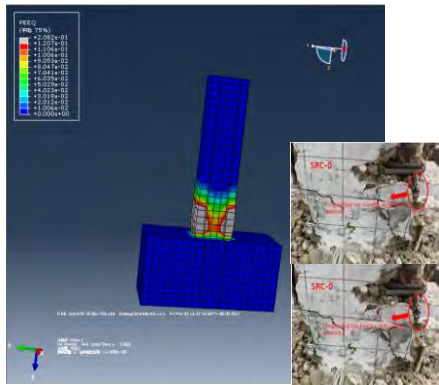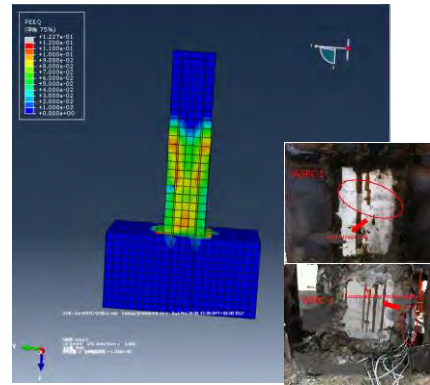
(a) SRC-0   (b) WSRC-0
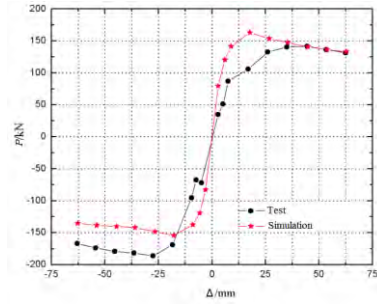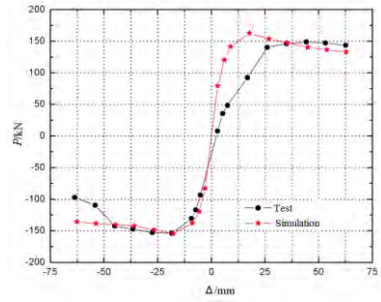
(c) WSRC-1   (d) WSRC-2

Fig .18. Comparison of P-Δ skeleton curves
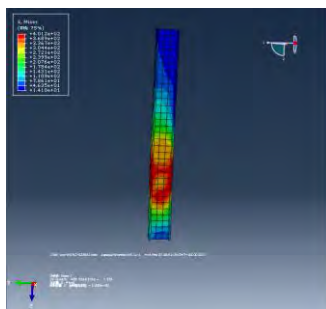

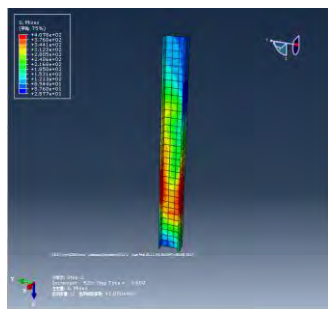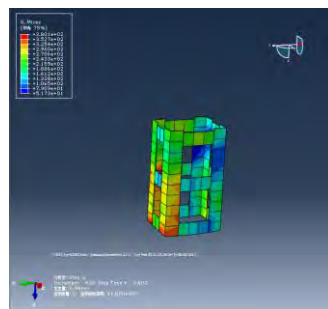(a) SRC-0   (b) WSRC-1

Fig .19. Comparison of concrete damage modes between FE analysis and experimental results

(a) SRC-0   (b) WSRC-1   (c) encased steel jacket

Fig .20. Profile steel and encased steel jacket damage modes

Comparison of finite element analysis result and test result on ultimate bearing capacity of the test specimen is shown in Table 4. The variation trend of ultimate bearing capacity by finite element analysis is consistent with practical test results i.e. ultimate bearing capacity, and ultimate bearing value of the reinforced test specimen decreases with the increase of seismic damage degree. The results of finite element analysis are larger than the experimental results, which is mainly due to the idealization of the simulation and errors existing in experimental test specimen material itself. Due to contribution of encased steel, ultimate bearing capacity of reinforced test specimen is larger than that of unreinforced test specimen. Compared with SRC-0, ultimate bearing capacity of test specimen WSRC-2 is increased by 10.81%, which indicates that reinforcement of encased steel jacket mainly improves ultimate bearing capacity of the test specimen. The results of the model are consistent with those of the test.

Table 4. Comparison of testing and simulation ultimate bearing capacities of composite steel-concrete columns

Specimen	Test ultimate bearing capacity/kN	Simulation ultimate bearing capacity/kN	Relative deviation
SRC-0	127.07	136.03	7.05%
WSRC-0	164.14	168.26	2.51
WSRC-1	148.04	156.38	5.63
WSRC-2	140.80	147.60	4.83

5.3. Specimens with different parameters

As mentioned in Section 2.1, the axial compression ratio applied to the 4 test specimens in this study is 0.32, which is due to the limited laboratory equipment capacity. In practice, the design of axial compression ratio is not fixed, neither is the reinforcement height of test specimen. In order to meet the actual needs, finite element analysis will be conducted on the above four aspects to complement deficiency of experimental results.

5.3.1. Specimens with different axial compression loads

In order to meet the real situation of high-rise buildings, two groups of axial compression ratio of the test specimens are added, 0.20 and 0.50 respectively, and its performance is studied by the above numerical model. The concrete strain cloud chart of the test specimen WSRC-0 is shown in Fig. 21. The long strain vector represents larger compressive deformation of the concrete. With the increase of n, main compressive strain of concrete increases obviously.
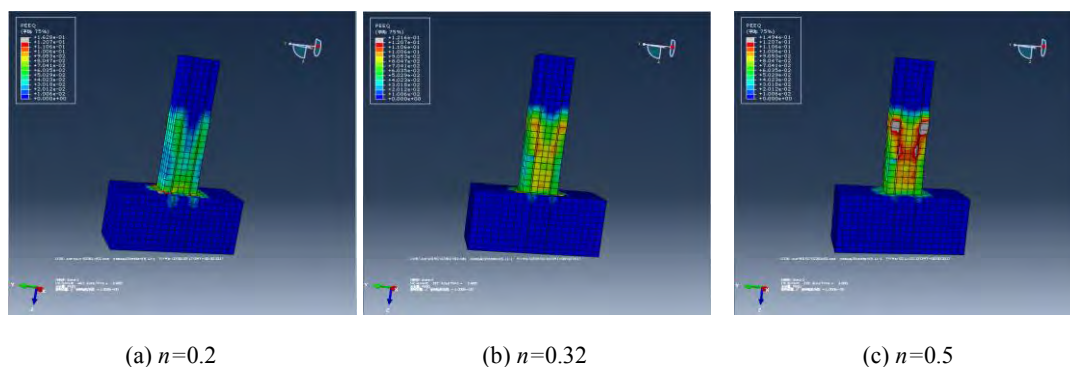

(a) $n=0.2$ (b) $n=0.32$ (c) $n=0.5$

Fig. 21. Strain nephogram of concrete

Comparison of ultimate bearing capacity, ultimate displacement and axial compression ratio of encased steel jacket-strengthened test specimen is shown in Fig. 22. With the increase of *n*, bearing capacity of the test specimens increases, while the displacement decreases. When *n* is the same, the bearing capacity and displacement of the reinforced test specimens decrease with the increase of seismic damage degree. Compared with the test specimens WSRC-0, when *n* is 0.20 and 0.50 respectively, the bearing capacity of test specimen WSRC-1 decreases by 7.50% and 6.59% respectively, and the displacement decreases by 5.50% and 7.89% respectively; the bearing capacity of WSRC-2 decreases by 12.81% and 10.99% respectively, and the displacement decreases by 16.51% and 20.00% respectively. The increasing rate of bearing capacity of the test specimen is slower than the decreasing rate of displacement, which indicates that increase of *n* is beneficial to structural resistance bearing, but not conducive to ductility and energy dissipation of the structure. The ultimate bearing capacity and ultimate displacement of the test specimens are sensitive to axial compression ratio.

5.3.2. Specimens with different strengthen height of encased steel jacket

In order to determine the reinforcement height of the cased steel jacket-strengthened test specimen, two reinforcement heights (750mm and 1000mm) were added based on the original heights, the performance was studied by the above numerical model. Taking WSRC-0 as an example, the strain cloud chart of the encased steel is shown in Fig. 22. The deformation of the encased steel does not increase with the increase of reinforcement length, and there is no deformation in the upper part of the cased steel with reinforcement height of 1000mm.
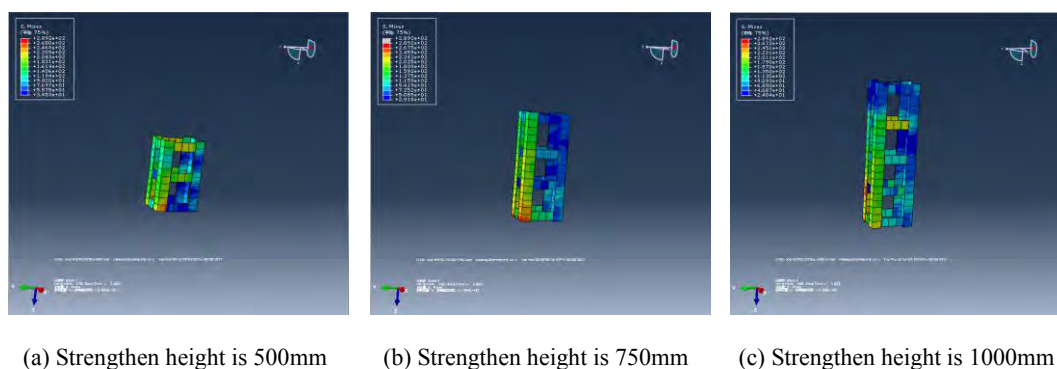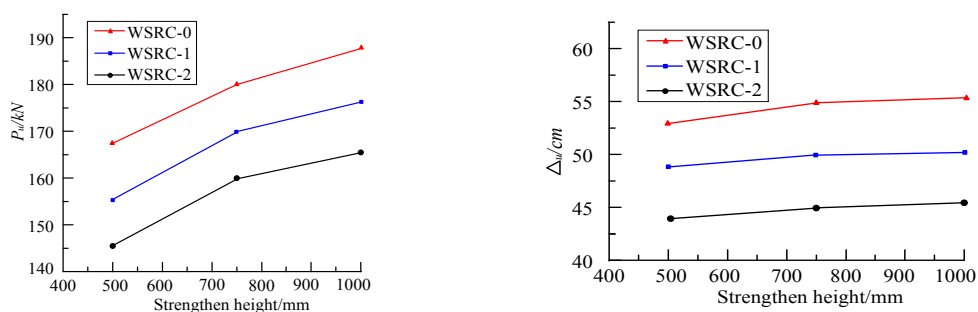

| (a) Strengthen height is 500mm | (b) Strengthen height is 750mm | (c) Strengthen height is 1000mm |

Fig. 22. Strain nephogram of encased steel jacket

Comparison of ultimate bearing capacity, ultimate displacement and reinforcement height of encased steel jacket-test specimens is shown in Fig. 23. With the increase of reinforcement height, the bearing capacity of the test specimens increases, and the displacement increases slightly. When the reinforcement height is the same, the bearing capacity and displacement of the reinforced test specimen decrease with the increase of seismic damage degree. Compared with the test specimen WSRC-0, when the reinforcement height is 750mm and 1000mm respectively, the bearing capacity of test specimen WSRC-1 decreases by 5.56% and 5.85% respectively, and the displacement decreases by 7.41% and 7.27% respectively; bearing capacity of test specimen WSRC-2 decreases by 11.11% and 11.70%, respectively, and displacement decreases by 14.81% and 14.55% respectively. The increasing rate of bearing capacity of the test specimen is slower than the decreasing rate of displacement, which indicates that increase of reinforcement height is beneficial to structural resistance bearing, but not conducive to ductility and energy dissipation of the structure.

The increase of ultimate load of the test specimen is more obvious when the reinforcement height is increasing from 500mm to 750mm, and the ultimate displacement is less sensitive to reinforcement height.

(a) Ultimate load at different strengthen height　　(b) Ultimate displacement at different strengthen height

Fig . 23. Strengthen height influenced the seismic behavior of specimens

6. Conclusions

In this test, the four test specimens were subjected to transverse cyclic loading test. The damage model, the force-displacement relation, the deformation ability, the strength and stiffness degradation and strain response of the test specimens were compared and analyzed. The finite element analysis was carried out and compared with the experimental results for verification. Numerical simulation was conducted to verify and evaluate mechanical properties of test specimens with different axial compression ratios and different reinforcement heights. The following conclusions can be drawn:

(1) It was observed that the damage development sequences of the four groups were similar. However, there were more cracks in the steel reinforced concrete comparative column (without damage and reinforcement). At the same time, steel reinforced concrete comparative column showed shear bending failure. Due to restraint effect of encased steel jacket, encased steel jacket-strengthened test specimen showed no shear yield.

(2) The cracks of encased steel jacket-strengthened steel reinforced concrete columns increased with the increase of seismic damage degree, which indicates that encased steel jacket-strengthened test specimen suppressed lateral burst of the concrete at the column foot and cannot fundamentally prevent increase of concrete cracks.

(3) Compared with the steel reinforced concrete comparative column, damage of encased steel jacket-strengthened test specimen was zero damage, moderate damage, severe damage, respectively, with ultimate load increased by 23.0%, 12.9% and 7.4%, respectively, and ultimate displacement increased by 23.7%, 12.4%, 8.0%, respectively. Due to the restraint effect of encased steel,the ultimate load and ultimate displacement of severely damaged test specimen strengthened with encased steel jacket exceeded that of original contrast test specimen, which is beneficial to improvement of seismic performance of the structure. However, the deformation capacities of core steel reinforced concrete parts of the four types were similar.

(4) Due to the lateral restraint effect of the concrete on steel reinforced concrete column, the role of welding head shear nail, and the stress of cross-configuration of rebar, stirrups and section steel the section steel did not yield during the whole loading process. From the results of finite element analysis, it can be seen that section steel simulated by different axial compression ratios and

different reinforcement heights did not yield.

(5) The finite element results showed that the increase of axial reinforcement ratio and reinforcement height was beneficial to the increase of bearing capacity of cased steel jacket-strengthened steel reinforced concrete column, wherein the ultimate displacement was particularly sensitive to axial compression ratio. The encased steel with reinforcement height of 1000 mm did not show deformation at its top part. However, as the reinforcement height increased from 500mm to 750mm, the bearing capacity of the test specimen was increased significantly, and the encased steel jacket was significantly deformed, which shows that the most favorable reinforcement height is 750mm. As encased steel jacket suppressed the transverse burst of concrete at the column foot, the compressive strain was smaller, and the shear failure of cased steel jacket-strengthened steel reinforced concrete column under high axial load was not easily affected.

Acknowledgements

References

[1] J.G. Teng, T. Yu, D. Fernando. Strengthening of steel structures with fiber-reinforced polymer composites. J. CONSTR. STEEL RES. 78 (2012) 131-143.

[2] C.X. Xu, B. Yang, B. Zhao, J.C. Zhang, W. Peng. Seismic performance of enveloped-steel-strengthened seismic-damaged CFST columns. Journal of Guangxi University (Nat Soi Ed) 40(4) (2015) 821-830.

[3] Z. Tao, Z.B. Wang, Q. Yu. Finite element modelling of concrete-filled steel stub columns under axial compression. J. CONSTR. STEEL RES. 89 (2013) 121-131.

[4] J.G. Nie, H.S. Hu, J.S. Fan, M.X. Tao, S.Y. Li, F.J. Liu. Experimental study on seismic behavior of high-strengthen concrete filled double-steel-plate composite walls. J. CONSTR. STEEL RES. 88 (2013) 206-219.

[5] T. Mohammed, B.H. Bakar, N.M. Bunnori. Torsional improvement of reinforced concrete beams using ultra high-performance fiber reinforced concrete (UHPFC) jackets-experimental study. CONSTR. BUILD. MATER. 106 (2016) 533-542

[6] L. Hussein, L. Amleh. Structural behavior of ultra-high performance fiber reinforced concrete-normal strength concrete or high strength concrete composite members. CONSTR. BUILD. MATER. 93 (2015) 1105-1116

[7] J. Song, Z.G. Gong, C.M. Zhu. Experiment study on seismic behavior of pre-damaged RC column strengthened with angle steel. Construction Technology 42(24) (2013) 24-27.

[8] A.S. Babatunde. Review of strengthening techniques for masonry using fiber reinforced polymers. CONSTR. BUILD. 161 (2017) 246-255.

[9] S. EI-Tawil, G.G. Deierlein. Strength and ductility of concrete encased composite columns. J. Struct. Eng. ASCE 125 (1999) 1009-1019.

[10] Q.Q. Xiong, Z.H. Chen, J.F. Kang, T. Zhou, W. Zhang. Experimental and finite element study on seismic performance of the LCFST-D columns. J. CONSTR. STEEL RES. 137 (2017) 119-134.

[11] P.F. Boyd, W.F. Cofer, D.I. Mclean. Seismic performance of steel-encased concrete columns under flexural loading. ACI Struct. J. 92(3) (1995) 355-364.

[12] L. Fang, B. Zhang, G.F. Jin, Z.L. Wang. Seismic behavior of concrete-encased steel cross-shaped columns. J. CONSTR. STEEL RES. 109 (2015) 24-33.

[13] E. Giménez, J.M. Adam, S. P.A. Calderón. Influence of strips configuration on the behavior of axially loaded RC columns strengthened by steel angles and strips. MATER. DESIGN 30(10) (2009) 4103-4111.

[14] P. Nagaprasad, D.R. Sahoo, D.C. Rai. Seismic strengthening of RC columns using external steel cage. EARTHQ ENG. STRUCT. D. 38(14) (2010) 1563-1586.

[15] J. Garzón-Roca, J. Ruiz-Pinilla, J.M. Adam, P.A. Calderón. An experimental study on steel-caged RC columns subjected to axial force and bending moment. ENG. STRUCT. 3(2) (2011) 580-590.

[16] ACI Committee 374. Guide for Testing Reinforced Concrete Structural Elements under Slowly Applied Simulated Seismic Loads. Farmington Hills, Michigan, USA: American Concrete Institute ACI 374 (2013) 2R-13.

[17] MOHURD (Ministry of Housing and urban-rural development of the People's Republic of China). Code for design of concrete structures (GB 50010-2010). China Architecture and Building Press: Beijing, China, (2011).

[18] S. Popovics. A numerical approach to the complete stress-strain curve of concrete. Cem. Concr. Res. 3 (1973) 583-599.

[19] A. Belarbi, T.T. Hsu. Constitutive laws of concrete in tension and reinforcing bars stiffened by concrete. ACI. Struct. J. 91 (1994) 465-474.

[20] V. Birtel, P. Mark. Parameterised finite element modelling of RC beam shear failure. In: Proceedings of the 19th Annual International ABAQUS Users' Conference. Boston, United States (2006) 95-108.

[21] X.P. Xu. Finite Element Analysis and Parametric Study of Reinforced Concrete Columns Strengthened with Bonded Steel. Institutes of Technology of South China, GuangDong (2015) .

[22] B.D. Scott, R. Park, M.J. Priestley. Stress-Strain Behavior of Concrete Confined by Overlapping Hoops at Low and High Strain Rates. ACI. STRUCT. J. 79(2) (1982) 13-27.

[23] M. Ryosuke, Y. Kentaro, T. Akira. Crack swarm inspection for estimation of crack location in carbon fiber reinforced plastics: A numerical study. COMPOS. STRUCT. 160 (2017) 36-42.

Highlights

- Lack of research on seismic behavior of steel reinforced concrete (SRC) frame column with seismic damage
- Study on strengthening methods of earthquake damaged steel reinforced concrete (SRC) frame columns
- The research on seismic performance of composite structures is beneficial to improve the seismic performance of structures
- Experimental and simulation methods are considered to make the conclusion more in line with the objective reality

This paper has the ability to resist earthquake damage again, and has good practical engineering value.